Space-based lidar measurements of global ocean carbon stocks

Michael J. Behrenfeld,[1] Yongxiang Hu,[2] Chris A. Hostetler,[2] Giorgio Dall'Olmo,[3] Sharon D. Rodier,[2] John W. Hair,[2] and Charles R. Trepte[2]

Received 31 July 2013; accepted 2 August 2013; published 23 August 2013.

[1] Global ocean phytoplankton biomass (C_{phyto}) and total particulate organic carbon (POC) stocks have largely been characterized from space using passive ocean color measurements. A space-based light detection and ranging (lidar) system can provide valuable complementary observations for C_{phyto} and POC assessments, with benefits including day-night sampling, observations through absorbing aerosols and thin cloud layers, and capabilities for vertical profiling through the water column. Here we use measurements from the Cloud-Aerosol Lidar with Orthogonal Polarization (CALIOP) to quantify global C_{phyto} and POC from retrievals of subsurface particulate backscatter coefficients (b_{bp}). CALIOP b_{bp} data compare favorably with airborne, ship-based, and passive ocean data and yield global average mixed-layer standing stocks of 0.44 Pg C for C_{phyto} and 1.9 Pg for POC. CALIOP-based C_{phyto} and POC data exhibit global distributions and seasonal variations consistent with ocean plankton ecology. Our findings support the use of spaceborne lidar measurements for advancing understanding of global plankton systems. **Citation:** Behrenfeld, M. J., Y. Hu, C. A. Hostetler, G. Dall'Olmo, S. D. Rodier, J. W. Hair, and C. R. Trepte (2013), Space-based lidar measurements of global ocean carbon stocks, *Geophys. Res. Lett.*, *40*, 4355–4360, doi:10.1002/grl.50816.

1. Introduction

[2] Passive "ocean color" remote sensing has revolutionized studies of global ocean ecology and carbon cycling [*McClain*, 2009; *Siegel et al*., 2013]. Sustaining climate-quality ocean color observations and advancing sensor spectral range and resolution capabilities remain satellite ocean science priorities. However, these passive measurements can only be made during daylight hours (optimally between ~10:00 and 14:00), are not reliable at low solar angles (e.g., high latitudes in winter), require cloud-free conditions, and are sensitive to atmospheric aerosols. Furthermore, developments in spectral inversion algorithms [e.g., *Maritorena et al*., 2002; *Lee et al*., 2002] have yielded critical new insights on ocean ecosystems [e.g., *Nelson and Siegel*, 2013; *Loisel et al*., 2001] and phytoplankton physiology [*Behrenfeld et al*., 2005; *Westberry et al*., 2008; *Behrenfeld et al*., 2008; *Siegel et al*., 2013] by simultaneously retrieving particulate backscattering, colored dissolved organic matter, and pigment absorption coefficients, but the accurate retrieval of these properties is limited by the information content within the measured ocean color bands. Finally, ocean color data provide limited information on depth-resolved plankton properties because the measured signal emanates from only the first attenuation length scale (i.e., approximately the depth of 10% incident light), exponentially weighted toward the surface.

[3] Light detection and ranging (lidar) systems have been deployed on ships and aircraft for characterizing ocean properties spanning from particulate attenuation and backscatter coefficients [*Dickey et al*., 2011], to phytoplankton pigments [*Hoge et al*., 1988], and even to zooplankton and fish stocks [*Churnside et al*., 2001; *Churnside and Thorne*, 2005; *Reese et al*., 2011]. As active sensors, lidar measurements have distinct advantages over passive retrievals for ocean observing, in that they can be conducted day or night, at low solar angles, through considerable aerosol loads and thin clouds, and can provide information on vertical structure in ecosystem properties. In terms of monitoring rapidly changing global plankton populations, lidar measurements simply cannot match the spatial coverage of passive systems. However, in conjunction with passive measurements, lidar data can provide important constraints for inversion algorithms, independent assessments of key ecosystem stocks, and complementary vertical profiling for interpreting ocean color data. Unfortunately, a lidar system specifically designed for ocean applications has never been flown in space. However, the National Aeronautics and Space Administration (NASA) and the Centre National d'Etudes Spatiales launched the Cloud-Aerosol Lidar and Infrared Pathfinder Satellite Observation (CALIPSO) satellite in 2006 as part of the A-train Earth Observing Sensor suite [*Winker et al*., 2009]. The primary instrument on CALIPSO is the Cloud-Aerosol Lidar with Orthogonal Polarization (CALIOP) sensor, and it has reliably collected global lidar measurements for the past 7 years. Because of its polarization characterization capabilities, CALIOP offers a unique opportunity for the first global evaluation of plankton properties from a space lidar.

[4] Here we focus on retrieving ocean particulate backscattering coefficients, b_{bp}, using CALIOP's 532 nm polarization channels. Two important ocean carbon stocks can be directly derived from b_{bp} data: total particulate organic carbon (POC) [*Loisel et al*., 2001; *Stramski et al*., 1999, 2008] and phytoplankton biomass (C_{phyto}) [*Behrenfeld et al*., 2005; *Westberry et al*., 2008; *Martinez-Vicente et al*., 2013]. Water column profiling capabilities with CALIOP are limited because the sensor was designed for atmospheric research and has a coarse in-water vertical resolution of 22.5 m. Our analysis therefore focuses on integrated b_{bp} estimates for the

Additional supporting information may be found in the online version of this article.

[1]Department of Botany and Plant Pathology, Oregon State University, Corvallis, Oregon, USA.
[2]NASA Langley Research Center, Hampton, Virginia, USA.
[3]Plymouth Marine Laboratory, Plymouth, UK.

Corresponding author: M. J. Behrenfeld, Department of Botany and Plant Pathology, Oregon State University, Cordley Hall 2082, Corvallis, OR 97331-2902, USA. (mjb@science.oregonstate.edu)

0094-8276/13/10.1002/grl.50816

first 22.5 m vertical bin below the ocean surface. However, our successful demonstration of b_{bp} retrievals implies that only minor modifications to a future ocean-focused lidar would be required to achieve appropriate profiling capabilities. As an initial validation of our approach, we compare CALIOP-based b_{bp} data with airborne lidar retrievals and ship-based optical measurements from a 2012 campaign in the Atlantic Ocean. We then compare our 6 year global CALIOP climatology with ocean color–based b_{bp} estimates from two state-of-the-art inversion algorithms and evaluate global seasonal patterns in CALIOP b_{bp}, POC, and C_{phyto} data.

2. Data and Methods

2.1. CALIOP Analysis

[5] Details on our analysis of CALIOP data and uncertainties in derived products are provided in Methods S1 in the supporting information (sections a and b). Briefly, assessment of ocean particulate backscatter from CALIOP's copolarization channel is extremely challenging because of signal contamination from surface reflection. The ocean signal measured by CALIOP's cross-polarization channel, however, is due almost entirely to backscatter from particulate matter. Retrievals of b_{bp} were therefore based on the cross-polarized component of column-integrated backscatter from below the ocean surface, β_{w+}. To account for variability in transmittance of the overlying atmosphere, β_{w+} was computed in terms of the column-integrated ratio of the copolarized and cross-polarized channels, δ_T (which includes surface and subsurface backscatter) (Methods S1). This ratio is independent of atmospheric transmittance and is very accurately calibrated. The value of β_{w+} is dependent on the column-integrated below-surface depolarization ratio, δ_w (which does not include surface backscatter). For the current analysis, δ_w was assigned a value of 0.1 (dimensionless) based on *Voss and Fry* [1984] and *Kokhanovsky* [2003]. Uncertainty in δ_w has some impact on errors in our derived b_{bp} values (Methods S1). The lidar surface backscatter, β_S, which is also required for calculating β_{w+}, was estimated using colocated Advanced Microwave Scanning Radiometer–EOS ocean surface wind speed measurements [*Hu et al*., 2008] for the period of June 2006 to September 2011. Microwave measurements of ocean surface backscatter from the CloudSat sensor [*Stephens et al*., 2002; *Tanelli et al*., 2008] were used to estimate β_S for the October 2011 to April 2012 period (Methods S1). Global seasonal maps of resultant CALIOP β_{w+} data are provided in Figure S1.

[6] To derive b_{bp} estimates comparable to field measurements, we first convert β_{w+} values into particulate backscatter coefficients at the 180° scattering angle, $b(\pi)$, using ocean downwelling diffuse attenuation coefficients (K_d) from Moderate Resolution Imaging Spectroradiometer (MODIS) at 532 nm (i.e., CALIOP's ocean-penetrating lidar emission wavelength) (Methods S1). Values of $b(\pi)$ at 532 nm were then related to b_{bp} at 440 nm using a mean $b(\pi)/b_{bp}$ value of 0.16 [*Fournier and Forand*, 1994; *Forand and Fournier*, 1999; *Chami et al*., 2006; *Sullivan and Twardowski*, 2009; *Whitmire et al*., 2010] and assuming a spectral slope of -1 for particulate backscattering [e.g., *Garver and Siegel*, 1997] (Methods S1). While sufficient for this first demonstration of b_{bp} retrievals from CALIOP, future refinements in the description of $b(\pi)/b_{bp}$ variability will be clearly beneficial. Finally, we removed CALIOP retrievals under the conditions of sea ice, extreme wind, or aerosol optical depths > 3 (Methods S1).

2.2. Field and Satellite Evaluation Data

[7] CALIOP $b_{bp}(440)$ data were evaluated by comparison with (1) field data collected during a 2012 Atlantic Meridional Transect (AMT22) cruise between 15 October (45°N, 20°W) and 24 October (22°N, 40°W) (Methods S1, sections c and d) and (2) MODIS-Aqua satellite ocean color b_{bp} products from the Garver-Siegel-Maritorena (GSM) inversion algorithm [*Garver and Siegel*, 1997; *Maritorena et al*., 2002; *Siegel et al*., 2002] and the Quasi-Analytical Algorithm (QAA) [*Lee et al*., 2002]. GSM and QAA data were from the NASA's Ocean Color website (http://oceancolor.gsfc.nasa.gov/).

[8] In support of this development effort toward satellite lidar retrievals of b_{bp}, NASA deployed an airborne high-spectral-resolution, dual-polarization lidar (HSRL-1) [*Hair et al*., 2008] during the AMT22 campaign. The HSRL-1 system was modified to achieve a vertical resolution in submarine particle profiles of 0.9 m at 532 nm and acquired data during overflights of the AMT22 ship track and for comparison with CALIOP retrievals. HSRL-1 measurements allow assessment of Brillouin scattering, depolarization ratios, and K_d, and, owing to high vertical resolution, accurate separation of surface and subsurface signals (Methods S1, section d). The HSRL-1 thus provided complementary lidar-based data that better constrain b_{bp} retrievals and permit evaluation of assumptions in the CALIOP approach.

[9] The various sources of b_{bp} data used in our comparison for the AMT campaign have different spatial and temporal resolutions, with these differences contributing to discrepancies in matchups. CALIOP is a nadir-only instrument (~100 m footprint) in a Sun-synchronous orbit (1:30 pm equator crossing time). Samples from adjacent orbits are separated by hundreds of kilometers. CALIOP and MODIS are both in the A-train constellation and thus acquire data within minutes from each other. However, MODIS has (1) different screening criteria applied before retrievals are made and (2) a wide swath, resulting in some space-time differences in MODIS and CALIOP data. CALIOP measurements were composited to a $2° \times 2°$ latitude-longitude grid, with grid cells intersecting the ship track being selected for comparison with in situ data. MODIS-Aqua GSM and QAA data intersecting the ship track are 9 km^2 resolution monthly mean products for October 2012. For ship b_{bp} measurements [*Dall'Olmo et al*. 2009], data integration times are equivalent to underway spatial scales of ~30 m and are acquired continuously along the ship track.

[10] Global climatological b_{bp} data from CALIOP, GSM, and QAA were used to estimate ocean mixed-layer stocks of POC and C_{phyto} using the algorithms of *Stramski et al*. [2008] and *Behrenfeld et al*. [2005], respectively. Mixed-layer depth (MLD) data were from www.science.oregonstate.edu/ocean.productivity and are based on the Fleet Numerical Meteorology and Oceanography Center model [*Clancy and Sadler*, 1992] and the Simple Ocean Data Assimilation model, where MLD was defined as the first depth at which density is 0.125 kg m^{-3} greater than the surface value.

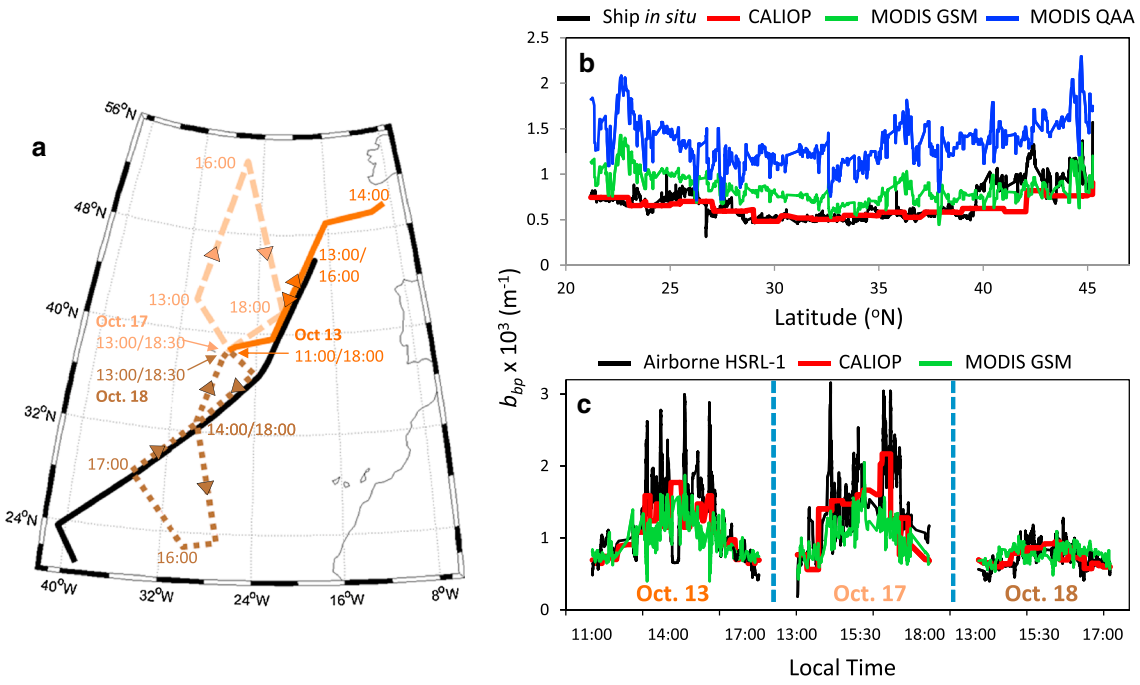

Figure 1. Particulate backscattering coefficients (b_{bp}) during the Atlantic Meridional Transect (AMT22) field campaign. (a) Black line = ship track. Solid orange, dashed peach, and dotted brown lines = aircraft tracks on 13, 17, and 18 October, respectively. Arrows indicate direction of flights, with approximate times shown in color according to date. (b) Comparison of b_{bp} values for in situ ship measurements (black), CALIOP retrievals (red), MODIS GSM product (green), and MODIS QAA product (blue). (c) Comparison of b_{bp} values for the three airborne campaigns. Black line = aircraft HSRL. Red = CALIOP. Green = MODIS GSM.

3. Results and Discussion

3.1. Comparison of b_{bp} Data for the North Atlantic

[11] Over the 10 day period of field measurements, the AMT22 ship track (Figure 1a, black line) transected mesotrophic to oligtrophic ocean environments, with shipboard b_{bp} values ranging from $>0.0016\ m^{-1}$ in the north to $\sim 0.0005\ m^{-1}$ toward the south (Figure 1b, black line). The spatial resolution of these ship-based measurements is far finer than that achieved with nearest-pixel, climatological average CALIOP data for October (Figure 1b, red line). Nevertheless, a correspondence ($R^2 = 0.54$) is still found between the lidar b_{bp} values and the in situ data, which is notable given the inherent challenges of matchup comparisons between satellite and in situ data [e.g., *Yuan et al.*, 2005].

[12] Overall, CALIOP retrievals tended to underestimate b_{bp} in the more productive northern region (in part reflecting the temporal mismatch between ship and CALIOP data for these highly variable northern waters), yielding a least squares regression relationship with a slope < 1 and an intercept of $0.0004\ m^{-1}$ (i.e., $b_{bp\text{-}CALIOP} = 0.374 b_{bp\text{-}SHIP} + 0.0004$; $R^2 = 0.54$) (Figure S2a). By comparison, satellite-based GSM b_{bp} estimates from October 2012 (Figure 1b, green line) were well matched with ship data in the northern region but overestimated b_{bp} in the south, relative to CALIOP matchup data. Overall, the GSM data gave a slightly lower regression slope and a lower coefficient of determination than CALIOP when compared to the in situ data and exhibited a greater regression intercept (i.e., $b_{bp\text{-}GSM} = 0.309 b_{bp\text{-}SHIP} + 0.0006$; $R^2 = 0.13$). Relative to GSM, the QAA results (Figure 1b, blue line) gave a slightly improved coefficient of determination when compared to ship b_{bp} data, as well as a regression slope closer to 1 than either the GSM or CALIOP comparisons (i.e., $b_{bp\text{-}QAA} = 0.684 b_{bp\text{-}SHIP} + 0.001$; $R^2 = 0.27$) (Figure S2b). However, the QAA data also exhibited a significant bias of $0.0007\ m^{-1}$ across the entire transect (Figure 1b).

[13] During AMT22, five successful airborne lidar measurement flights were completed. We focus here on the flights of October 13th, 17th, and 18th (orange, peach, and brown lines in Figure 1a, respectively). These airborne transects were selected to maximize clear-sky conditions, to overpass the ship transect line, and to underfly coincident CALIOP orbits. Comparison of HSRL b_{bp} retrievals with QAA estimates again indicated a significant bias in the QAA data of $0.0006\ m^{-1}$ at HSRL-based b_{bp} values less than 0.0015 (Figure S3). By comparison, GSM data (Figure 1c, green line) showed a better correspondence to HSRL-based data (Figure 1c, black line) across the full range of b_{bp} values for the three airborne campaigns, with an overall coefficient of determination of $R^2 = 0.39$. If anything, the GSM retrievals are slightly lower than HSRL-based estimates at high b_{bp} values. Of the three data sources, the CALIOP results exhibited the closest agreement with HSRL data ($b_{bp\text{-}CALIOP} = 0.537 b_{bp\text{-}HSRL} + 0.0004$; $R^2 = 0.58$) and reasonable agreement with GSM data ($b_{bp\text{-}CALIOP} = 0.875 b_{bp\text{-}GSM} + 0.0002$; $R^2 = 0.31$).

[14] Results from these field-based evaluations demonstrate the capacity of CALIOP for quantitatively detecting b_{bp} from below-surface ocean particles, with retrieved b_{bp} values within the range of variability associated with alternative ocean color–based algorithms. This success justifies a preliminary examination of global CALIOP b_{bp} data.

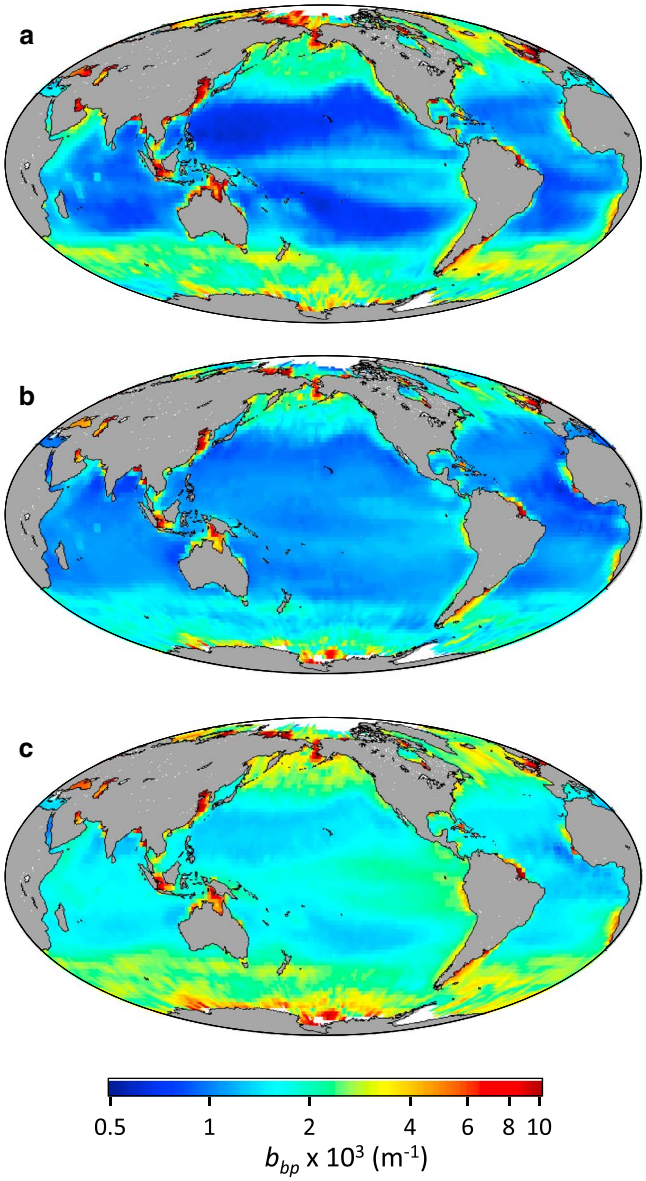

Figure 2. Global distributions of surface particulate backscattering coefficients (b_{bp}). (a) CALIOP-based b_{bp}. (b) MODIS-based b_{bp} from the GSM algorithm. (c) MODIS-based b_{bp} from the QAA algorithm. Data in each panel are climatological annual averages for the 2006–2012 period. All data have been standardized to 2° latitude × 2° longitude pixels.

3.2. Global CALIOP b_{bp} and Ocean Carbon Stocks

[15] Phytoplankton production fuels mixed-layer plankton communities, with an average turnover time for the global phytoplankton on the order of 2–6 days [*Behrenfeld and Falkowski*, 1997]. Accordingly, the global open-ocean distribution of phytoplankton biomass (C_{phyto}) is qualitatively similar to that of total particulate organic carbon (POC). This spatial variability in suspended particle loads directly impacts light scattering properties in the surface ocean, allowing optically based assessments of POC [e.g., *Loisel et al*., 2001; *Stramski et al*., 2008; *Cetinić et al*., 2012] and C_{phyto} [*Behrenfeld and Boss*, 2003, 2006; *Behrenfeld et al*., 2005]. Over most of the permanently stratified ocean (roughly between 40°N and 40°S latitudes) [*Behrenfeld et al*., 2006], C_{phyto} and POC concentrations are relatively low and stable over the annual cycle [*Siegel et al*., 2013]. In upwelling systems, monsoon regions, and at high latitudes where physical processes significantly disturb ecosystem balances [*Behrenfeld et al*., 2013] and enhance surface nutrient loads [*Sverdrup*, 1955], strong seasonal cycles in C_{phyto} and POC may be observed. Accordingly, this spatial and seasonal variability in plankton stocks should be apparent in global patterns of b_{bp}.

[16] Combining all CALIOP b_{bp} data for our 2006–2012 analysis period yields a global climatology that exhibits all the anticipated major ocean plankton features (Figure 2a). Elevated b_{bp} values in the subarctic Atlantic reflect the region's large spring bloom, while somewhat lower average values are found in the seasonally iron-limited subarctic Pacific. Patchy blooms in the Southern Ocean are also reflected in the CALIOP b_{bp} data and correspond to varying sources of surface iron. Likewise, the permanently stratified oceans have the diminished values of b_{bp} expected for these low-nutrient, low-biomass waters, except in regions of upwelling (e.g., equatorial Pacific) (Figure 2a). Climatologies of b_{bp} data for the Boreal summer (June–August) (Figure 3a) and Boreal winter (December–February) (Figure 3b) further illustrate the strong seasonality of high-latitude plankton stocks and, again, demonstrate the feasibility of characterizing below-surface ocean particle stocks and their variability with a space-based lidar.

[17] Compared to CALIOP data, the 2006–2012 global climatology of GSM b_{bp} data shows diminished high-latitude blooms but comparable values in lower-latitude oligotrophic

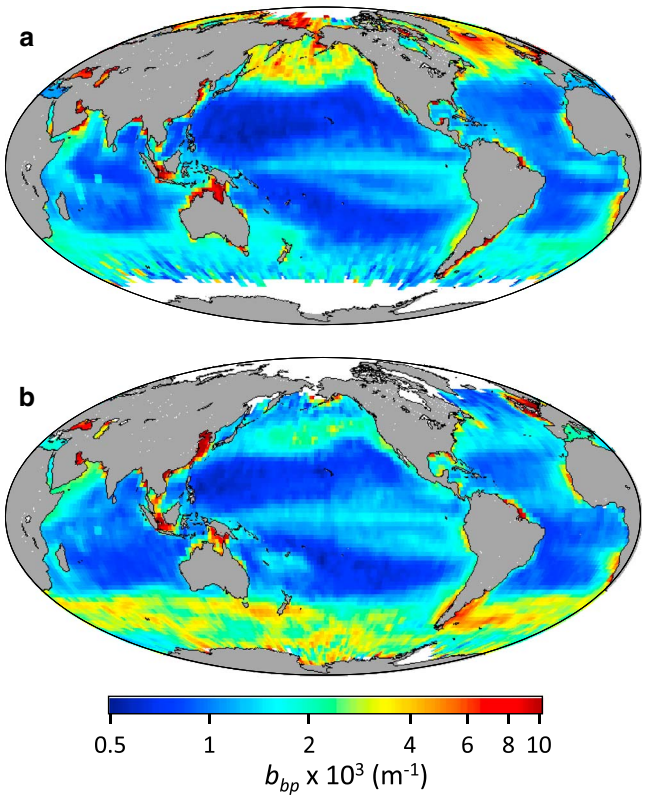

Figure 3. Seasonal changes in surface particulate backscattering coefficients (b_{bp}). (a) Boreal summer (June–August). (b) Boreal winter (December–February). Data are CALIOP-based b_{bp} seasonal average climatologies for the 2006–2012 period. Data are binned to 2° latitude × 2° longitude pixels.

regions (Figure 2b). For the same period, the QAA climatology gives similar-magnitude high-latitude blooms as CALIOP but significantly elevated b_{bp} values in clearer waters (Figure 2c), consistent with our field-based results (Figures 1b and S3). Overall, the global distribution of CALIOP b_{bp} values is consistent with many features in the GSM and QAA retrievals and well within the range of uncertainty between these two passive ocean color–based algorithms.

[18] Using published relationships based on b_{bp} [*Stramski et al*., 2008; *Behrenfeld et al*., 2005, respectively], CALIOP data yield POC and C_{phyto} values that range from minima of <30 and <4 mg C m^{-3} to maxima of >450 and >150 mg C m^{-3}, respectively, with global total mixed-layer stocks of 1.9 Pg for POC and 0.44 Pg for C_{phyto}. For GSM data, POC values range from <28 to >350 mg C m^{-3} and C_{phyto} values from <3 to >100 mg C m^{-3}, with lower estimated global mixed-layer stocks of 1.5 Pg for POC and 0.33 Pg for C_{phyto}. Conversely, QAA data give larger global mixed-layer stocks of 2.2 Pg for POC and 0.56 Pg for C_{phyto}, with POC ranging from <45 to >400 mg C m^{-3} and C_{phyto} from <8 to >120 mg C m^{-3}.

[19] CALIOP-based carbon ranges and total inventories fall between those calculated from GSM and QAA data. Figure S4 shows frequency distributions of POC for CALIOP, GSM, QAA, and the MODIS standard POC product. CALIOP data show (1) a dual-mode frequency distribution similar to QAA, but with peaks at lower POC concentrations; (2) a low-POC peak (~45 mg C m^{-3}) consistent with the peak in GSM data; and (3) an overall distribution that is most similar to the MODIS product (Figure S5), although lacking the values below ~30 mg C m^{-3}) (Figure S4). This latter finding is somewhat surprising since, unlike the other three approaches, the MODIS POC values are calculated using a wave band ratio algorithm, rather than b_{bp}.

4. Conclusions

[20] Results presented here demonstrate the quantitative measurement of ocean particles with a space-based lidar. CALIOP b_{bp} retrievals allow independent assessments of mixed-layer carbon stocks and provide a globally comprehensive data set for algorithm development, thus addressing the paucity and spatial bias of in situ data. With only a modest improvement in technology (e.g., improved vertical resolution and effective separation of particulate and Brillouin scattering components, as achieved with HSRL-1), our findings suggest that the combination of an ocean-focused satellite lidar and passive ocean color sensor could soon yield three-dimensional global reconstructions of upper ocean plankton ecosystems.

[21] **Acknowledgments.** This research was supported by funding from NASA's Ocean Biology and Biogeochemistry Program, the Aerosols-Clouds-Ecosystems Science Working Group, and the CALIPSO mission. We thank Robert O'Malley for assistance with data analysis, Toby Westberry for manuscript comments, and the CALIPSO team for CALIOP data analysis support. This study is a contribution to the international IMBER project, and ship-based measurements were in part supported by the UK Natural Environment Research Council National Capability funding to Plymouth Marine Laboratory and the National Oceanography Centre, Southampton. This is contribution number 234 of the AMT programme.

[22] The Editor thanks one anonymous reviewer for assistance evaluating this manuscript.

References

Behrenfeld, M. J., and E. Boss (2003), The beam attenuation to chlorophyll ratio: an optical index of phytoplankton physiology in the surface ocean?, *Deep Sea Res., Part I*, *50*, 1537–1549.

Behrenfeld, M. J., and E. Boss (2006), Beam attenuation and chlorophyll concentration as alternative optical indices of phytoplankton biomass, *J. Mar. Res.*, *64*, 431–451.

Behrenfeld, M. J., and P. G. Falkowski (1997), Photosynthetic rates derived from satellite-based chlorophyll concentration, *Limnol. Oceanogr.*, *42*, 1–20.

Behrenfeld, M. J., E. Boss, D. A. Siegel, and D. M. Shea (2005), Carbon-based ocean productivity and phytoplankton physiology from space, *Global Biogeochem. Cycles*, *19*, GB1006, doi:10.1029/2004GB002299.

Behrenfeld, M. J., R. O'Malley, D. A. Siegel, C. McClain, J. Sarmiento, G. Feldman, A. Milligan, P. Falkowski, R. Letelier, and E. Boss (2006), Climate-driven trends in contemporary ocean productivity, *Nature*, *444*, 752–755.

Behrenfeld, M. J., K. Halsey, and A. Milligan (2008), Evolved physiological responses of phytoplankton to their integrated growth environment, *Philos. Trans. R. Soc. B*, *363*, 2687–2703, doi:10.1098/rstb.2008.0019.

Behrenfeld, M. J., S. C. Doney, I. Lima, E. S. Boss, and D. A. Siegel (2013), Annual cycles of ecological disturbance and recovery underlying the subarctic Atlantic spring plankton bloom, *Global Biogeochem. Cycles*, *27*, 526–540, doi:10.1002/gbc.20050.

Cetinić, I., M. J. Perry, N. T. Briggs, E. Kallin, E. A. D'Asaro, and C. M. Lee (2012), Particulate organic carbon and inherent optical properties during 2008 North Atlantic Bloom Experiment, *J. Geophys. Res.*, *117*, C06028, doi:10.1029/2011JC007771.

Chami, M., E. B. Shybanov, G. A. Khomenko, M. E.-G. Lee, O. V. Martynov, and G. K. Korotaev (2006), Spectral variation of the volume scattering function measured over the full range of scattering angles in a coastal environment, *Appl. Opt.*, *45*, 3605–3619.

Churnside, J. H., and R. E. Thorne (2005), Comparison of airborne lidar measurements with 420 kHz echo-sounder measurements of zooplankton, *Appl. Opt.*, *44*, 5504–5511.

Churnside, J. H., K. Sawada, and T. Okumura (2001), A comparison of airborne lidar and echo sounder performance in fisheries, *J. Mar. Acoust. Soc. Jpn.*, *28*, 175–183.

Clancy, R. M., and W. D. Sadler (1992), The fleet numerical oceanography center suite of oceanographic models and products, *Weather Forecast.*, *7*, 307–327.

Dall'Olmo, G., T. K. Westberry, M. J. Behrenfeld, E. Boss, and W. H. Slade (2009), Significant contribution of large particles to optical backscattering in the open ocean, *Biogeosciences*, *6*, 947–967.

Dickey, T. D., G. W. Kattawar, and K. J. Voss (2011), Shedding new light on light in the ocean, *Phys. Today*, *64*, 44–49.

Forand, J. L., and G. R. Fournier (1999), Particle distribution and index of refraction estimation for Canadian waters, *Proc. SPIE*, *3761*, 34–44.

Fournier, G. R., and J. L. Forand (1994), Analytic phase function for ocean water, *Proc. SPIE*, *2258*, 194–201.

Garver, S. A., and D. A. Siegel (1997), Inherent optical property inversion of ocean color spectra and its biogeochemical interpretation: I. Time series from the Sargasso Sea, *J. Geophys. Res.*, *102*, 18,607–18,625.

Hair, J. W., C. A. Hostetler, A. L. Cook, D. B. Harper, R. A. Ferrare, T. L. Mack, W. Welch, L. R. Izquierdo, and F. E. Hovis (2008), Airborne high spectral resolution lidar for profiling aerosol optical properties, *Appl. Opt.*, *47*, 6734–6752.

Hoge, F. E., C. W. Wright, W. B. Krabill, R. R. Buntzen, G. D. Gilbert, R. N. Swift, J. K. Yungel, and R. E. Berry (1988), Airborne lidar detection of subsurface oceanic scattering layers, *Appl. Opt.*, *27*, 3969–3977.

Hu, Y., et al. (2008), Sea surface wind speed estimation from space-based lidar measurements, *Atmos. Chem. Phys.*, *8*, 3593–3601.

Kokhanovsky, A. A. (2003), Parameterization of the Mueller matrix of oceanic waters, *J. Geophys. Res.*, *108*(C6), 3175, doi:10.1029/2001JC001222.

Lee, Z. P., K. L. Carder, and R. A. Arnone (2002), Deriving inherent optical properties from water color: A multi-band quasi-analytical algorithm for optically deep waters, *Appl. Opt.*, *41*, 5755–5772.

Loisel, H., E. Bosc, D. Stramski, K. Oubelkheir, and P.-Y. Deschamps (2001), Seasonal variability of the backscattering coefficient in the Mediterranean Sea on Satellite SeaWiFS imagery, *Geophys. Res. Lett.*, *28*, 4203–4206.

Maritorena, S., D. A. Siegel, and A. R. Peterson (2002), Optimization of a semianalytical ocean color model for global-scale applications, *Appl. Opt.*, *41*, 2705–2714.

Martinez-Vicente, V., G. Dall'Olmo, G. Tarran, E. Boss, and S. Sathyendranath (2013), Optical backscattering is correlated with phytoplankton carbon across the Atlantic Ocean, *Geophys. Res. Lett.*, *40*, 1154–1158, doi:10.1002/grl.50252.

McClain, C. R. (2009), A decade of satellite ocean color observations, *Annu. Rev. Mar. Sci.*, *1*, 19–42.

Nelson, N. B., and D. A. Siegel (2013), The global distribution and dynamics of chromophoric dissolved organic matter, *Annu. Rev. Mar. Sci.*, *5*, 447–476.

Reese, D. C., R. T. O'Malley, R. D. Brodeur, and J. H. Churnside (2011), Epipelagic fish distributions in relation to thermal fronts in a coastal upwelling system using high-resolution remote-sensing techniques, *ICES J. Mar. Sci.*, *68*, 1865–1874.

Siegel, D. A., S. Maritorena, N. B. Nelson, D. A. Hansell, and M. Lorenzi-Kayser (2002), Global distribution and dynamics of colored dissolved and detrital organic materials, *J. Geophys. Res.*, *107*(C12), 3228, doi:10.1029/2001JC000965.

Siegel, D. A., et al. (2013), Regional to global assessments of phytoplankton dynamics from the SeaWiFS mission, *Remote Sens. Environ.*, *135*, 77–91.

Stephens, G. L., et al. (2002), The CloudSat mission and the A-train, *Bull. Am. Meteorol. Soc.*, *83*, 1771–1790.

Stramski, D., R. A. Reynolds, M. Kahru, and B. G. Mitchell (1999), Estimation of particulate organic carbon in the ocean from satellite remote sensing, *Science*, *285*, 239–242, doi:10.1126/science.285.5425.239.

Stramski, D., et al. (2008), Relationships between the surface concentration of particulate organic carbon and optical properties in the eastern South Pacific and eastern Atlantic Oceans, *Biogeosciences*, *5*, 171–201, doi:10.5194/bg-5-171-2008.

Sullivan, J. M., and M. S. Twardowski (2009), Angular shape of the oceanic particulate volume scattering function in the backward direction, *Appl. Opt.*, *48*, 6811–6819.

Sverdrup, H. U. (1955), The place of physical oceanography in oceanographic research, *J. Mar. Res.*, *14*, 287–294.

Tanelli, S., S. L. Durden, E. Im, K. S. Pak, D. G. Reinke, P. Partain, J. M. Haynes, and R. T. Marchand (2008), CloudSat's cloud profiling radar after two years in orbit: Performance, calibration, and processing, *IEEE Trans. Geosci. Remote Sens.*, *46*, 3560–3573.

Voss, K., and E. Fry (1984), Measurement of the Mueller matrix for ocean water, *Appl. Opt.*, *23*, 4427–4436.

Westberry, T. K., M. J. Behrenfeld, D. A. Siegel, and E. Boss (2008), Carbon-based primary productivity modeling with vertically resolved photoacclimation, *Global Biogeochem. Cycles*, *22*, GB2024, doi:10.1029/2007GB003078.

Whitmire, A. L., W. S. Pegau, L. Karp-Boss, E. Boss, and T. J. Cowles (2010), Spectral backscattering properties of marine phytoplankton cultures, *Opt. Express*, *18*, 15,073–15,093.

Winker, D. M., M. A. Vaughan, A. Omar, Y. X. Hu, K. A. Powell, Z. Y. Liu, W. H. Hunt, and S. A. Young (2009), Overview of the CALIPSO Mission and CALIOP data processing algorithms, *J. Atmos. Oceanic Technol.*, *26*, 2310–2323.

Yuan, J., M. Dagg, and C. Del Castillo (2005), In pixel variations of chl a fluorescence in Northern Gulf of Mexico and their implications for calibrating remotely sensed chl a and other products, *Cont. Shelf Res.*, *25*, 1894–1904.